nature communications

Article

https://doi.org/10.1038/s41467-025-63358-6

Dielectric strength weakening of hexagonal boron nitride nanosheets under mechanical stress

Received: 2 November 2024

Accepted: 14 August 2025

Published online: 29 August 2025

Check for updates

Bingjie Wang[1], Chuanli Yu[2], Yifan Jiang[1], Chong Tian[3], Jiamin Tian[1], Shuo Li[1], Zheng Fang[1], Menglan Li[1,4], Weilong Wu[1], Zhaohe Dai[2], Takashi Taniguchi[5], Kenji Watanabe[6], Qing Chen[1] & Xianlong Wei[1]

Hexagonal boron nitride (hBN) nanosheets have become the most promising candidates as gate dielectric and insulating substrates for two-dimensional (2D) material-based electronic and optoelectronic devices. While mechanical stress in hBN nanosheets is often either intrinsically or intentionally introduced for 2D material-based devices during device fabrication and operation, the dielectric strength of hBN nanosheets under mechanical stress is still elusive. In this work, the dielectric strength of hBN nanosheets in a metal/hBN/metal structure is systematically studied when mechanical stress normal to nanosheets is applied. The dielectric strength of hBN nanosheets is found to be weakened with lower breakdown strength, shorter breakdown time, and larger leakage current under the mechanical stress with the order of 100 MPa, and the weakening is more remarkable for thinner nanosheets. The thickness-dependent weakening of dielectric strength is attributed to the thickness-dependent stress gradient in hBN nanosheets. Furthermore, the ability of hBN nanosheets to block leakage current can be significantly degraded by mechanical stress even for thick nanosheets up to 41.3 nm. The results indicate that it is highly important to eliminate mechanical stress in high-performance 2D material-based devices employing hBN nanosheets as 2D insulators.

Hexagonal boron nitride (hBN) nanosheets are considered the most promising two-dimensional (2D) insulator and are used as gate dielectric[1,2], insulating substrates[3,4], insulating barrier[5,6] and encapsulation layers[7–10] for 2D material-based electronic and optoelectronic devices. Due to the atomically smooth interface that is relatively free of dangling bonds and charge traps in hBN/2D material heterostructures[3], field-effect transistors with graphene and 2D semiconductor channels show boosted performances, including ultrahigh carrier mobility, ultralow charge inhomogeneity, and ultralong mean free paths if the channel is supported or encapsulated by high-quality hBN nanosheets[2,6,8,11]. Furthermore, hBN encapsulation can be used to preserve the intrinsic physical properties of 2D materials. For example, superconductivity in magic-angle graphene and Mott insulator in trilayer graphene were observed with hBN encapsulation[9,10]. As a 2D insulator, hBN nanosheets therefore play important roles in achieving high-performance 2D material-based devices and revealing unique physical phenomena related to 2D materials.

[1]Key Laboratory for the Physics and Chemistry of Nanodevices, School of Electronics, Peking University, Beijing, China. [2]Department of Mechanics and Engineering Science, College of Engineering, Peking University, Beijing, China. [3]State Key Laboratory for Artificial Microstructures and Mesoscopic Physics, School of Physics, Peking University Yangtze Delta Institute of Optoelectronics, Peking University, Beijing, China. [4]Academy for Advanced Interdisciplinary Studies, Peking University, Beijing, China. [5]Research Center for Materials Nanoarchitectonics, National Institute for Materials Science, Tsukuba, Japan. [6]Research Center for Electronic and Optical Materials, National Institute for Materials Science, Tsukuba, Japan. e-mail: weixl@pku.edu.cn

Mechanical deformation with stress generally in the range of 0–1000 MPa usually accompanies the fabrication and operation of the devices reliant on hBN/2D material heterostructures, particularly state-of-the-art electronic devices like stacked nanosheet gate-all-around (GAA) field effect transistors (FETs)[12], vertical-transport FETs (VTFETs)[13], 2D flexible/strain FETs[14] and flexible neuromorphic devices[15]. To date, most 2D FETs based on hBN dielectric layers still rely on mechanical transfer and stacking procedure[16–18]. Deformations in the forms of wrinkles, bubbles, and buckling are commonly observed in transferred 2D materials[19], so it is difficult to construct hBN/2D material heterostructures free of mechanical stress, especially for large-area construction. Furthermore, the difference in thermal expansion coefficient between hBN and its surrounding materials was found to induce irreversible straining in hBN nanosheets when heated[20,21]. Mechanical stress in hBN is therefore introduced if it is treated by thermal annealing, which is a general procedure in fabricating hBN/2D material heterostructures and their devices[11]. Moreover, in most of the studies in advanced electronic devices involving 3D stacked architectures like GAA, structure-induced strain is widely present[22], and the variation of the intrinsic dielectric strength of hBN as a stacked part is usually ignored. Finally, due to the atomic thickness with high flexibility, hBN nanosheets have already been explored for use as insulating substrates and encapsulation layers for 2D material-based flexible devices, where mechanical stress in hBN is inevitable during device preparation and operation[23,24]. Dielectric strength of hBN under mechanical stress is therefore highly important for developing 2D material-based devices.

Mechanical stress-induced dielectric strength weakening of conventional silicon dioxide (SiO_2) or other dielectric films is well studied[25,26], whereas that of 2D hBN nanosheets has not been studied. The elusive dielectric strength of hBN nanosheets under mechanical stress is mainly attributed to the challenges of the simultaneous and reliable determination of its dielectric strength and mechanical stress in experiments. A few experimental methods, including electrical measurements on stretchable substrates[27] and indentation tests with conductive atomic force microscopy (C-AFM) probes[28], were developed to perform simultaneous electrical and mechanical measurements on ultrathin 2D materials. While the dielectric strength of polymers (i.e. polyimide, polyethylene terephthalate, etc.) used for stretchable substrates is generally smaller than that of hBN[29,30], the dielectric strength of hBN cannot be tested on these stretchable substrates. As for indentation with AFM probes, it is hard to accurately determine the indented area and mechanical stress because of the complex contact mechanics of sharp AFM probes[31,32]. More importantly, AFM tests are generally performed at atmospheric pressure, which makes the electrical contact between the AFM probe and 2D materials ambiguous and unstable because of reactive interfacial water and oxygen molecules, especially when dense electrical current passes through the contact[33,34]. Despite the challenge of AFM indentation tests, C-AFM has been applied to study dielectric breakdown of hBN without intended mechanical stress. Several important phenomena have been observed in dielectric breakdown of hBN, including layer-by-layer breakdown[35,36], non-volatile resistive switch[37], B-vacancy-dominated defect mechanisms[38], interlayer molecular bridges[39], electrode-affected leakage current[40], and so on.

In this work, the dielectric strength of hBN nanosheets under mechanical stress is systematically studied by an in situ scanning electron microscopy (SEM) method. With the method, the dielectric strength of hBN nanosheets in a metal/hBN/metal structure is systematically measured when well-determined mechanical stress normal to nanosheets is applied. Dielectric strength weakening of hBN nanosheets is observed to show lower breakdown strength, shorter breakdown time, and larger leakage current prior to breakdown when they are subjected to normal mechanical stress with the order of 100 MPa. The results indicate that it is highly important to eliminate mechanical stress in high-performance 2D material-based devices employing hBN nanosheets as 2D insulators.

Results and discussion

Dielectric strength weakening in ramped voltage stress tests

High-quality hBN nanosheets mechanically exfoliated from bulk hBN crystals are used in this work (see Fig. S1 for structural characterization of hBN nanosheets). To facilitate multiple dielectric strength measurements on hBN nanosheets with the same thickness, large hBN nanosheets with uniform thickness are first transferred onto a SiO_2/Si substrate with an Au/Ti coating film, and an array of 1 μm wide circular islands in the structure of metal/hBN/metal are then fabricated from the nanosheets (see Figs. 1a, and S2 for device structure and fabrication). Dielectric strength measurements are performed at room temperature and inside the vacuum chamber of an SEM (see Fig. S3 for more details of the experimental setup). The substrate with metal/hBN/metal islands is fixed to a spring stage that is used to measure the force applied to the islands (Fig. 1b). To measure the dielectric strength of hBN nanosheets under normal mechanical stress, a tungsten (W) electrical probe with a radius of ~200 nm is manipulated to indent the top metal layer of an island and measure the electrical current across the metal/hBN/metal structure under an applied voltage (see Fig. 1c and Supplementary Movie 1). The compression force applied to hBN nanosheets is obtained through the formula $F = kd$, where k is the elastic coefficient of the spring stage (see Fig. S4 in Supplementary Information), and d is the retraction distance of the substrate that can be directly measured by SEM imaging. Due to the bending stiffness of the top metal layer, the indented area S of the hBN nanosheets is larger than that of the indenter with a nonuniform stress distribution. According to our recent work[41,42], a well-determined apparent normal stress (σ) can be obtained by finite element simulation (FEM) (see Fig. S5 in Supplementary Information). Dielectric strength and normal mechanical stress of hBN nanosheets can therefore be well and simultaneously determined in our experiments.

The dielectric strength of hBN nanosheets is firstly studied by ramped voltage stress (RVS) tests, where the electrical current across the metal/hBN/metal structure is recorded while increasing the applied voltage linearly with time until dielectric breakdown. Each current (I)–voltage (V) curve is measured from a different island sample without any previous measurements (referred to as multi-sample RVS tests), which enables us to exclude the possible memory effects of previous measurements. To investigate the effect of thickness on the dielectric strength of hBN nanosheets, the dielectric strength of hBN nanosheets with thicknesses in the range of about 5–40 nm is studied (see Fig. S6 for thickness measurements by AFM imaging). Figure 1d shows the typical I–V curves of hBN nanosheets with three different thicknesses (4.6, 11.5 and 41.3 nm) under zero normal mechanical stress. The curves show a common feature that obvious leakage current is observed at a voltage (V_{LC}) before the dielectric breakdown of hBN nanosheets at a larger voltage (V_{BD}), where leakage current experiences a sudden jump. Breakdown strength (E_{BD}) is therefore obtained by $E_{BD} = V_{BD}/t_{BN}$, where t_{BN} is the thickness of the hBN nanosheets. The strength of the electric field corresponding to V_{LC} is defined as $E_{LC} = V_{LC}/t_{BN}$. The voltage interval between V_{LC} and V_{BD} is usually regarded as the stage of progressive breakdown of hBN nanosheets, in which defects are randomly generated and the leakage current increases quickly. For thick nanosheets with 41.3 nm thickness, the leakage current shows a progressive increase with the voltage until breakdown. In contrast, the leakage current of thin nanosheets with 4.6 and 11.5 nm thicknesses is highly fluctuating with less dependence on voltage before breakdown. The above breakdown behaviors observed at zero stress agree well with those observed in previous C-AFM experiments[28,43].

What will happen if hBN is subjected to mechanical stress while resisting the external electric field? To investigate the effects of

https://doi.org/10.1038/s41467-025-63358-6

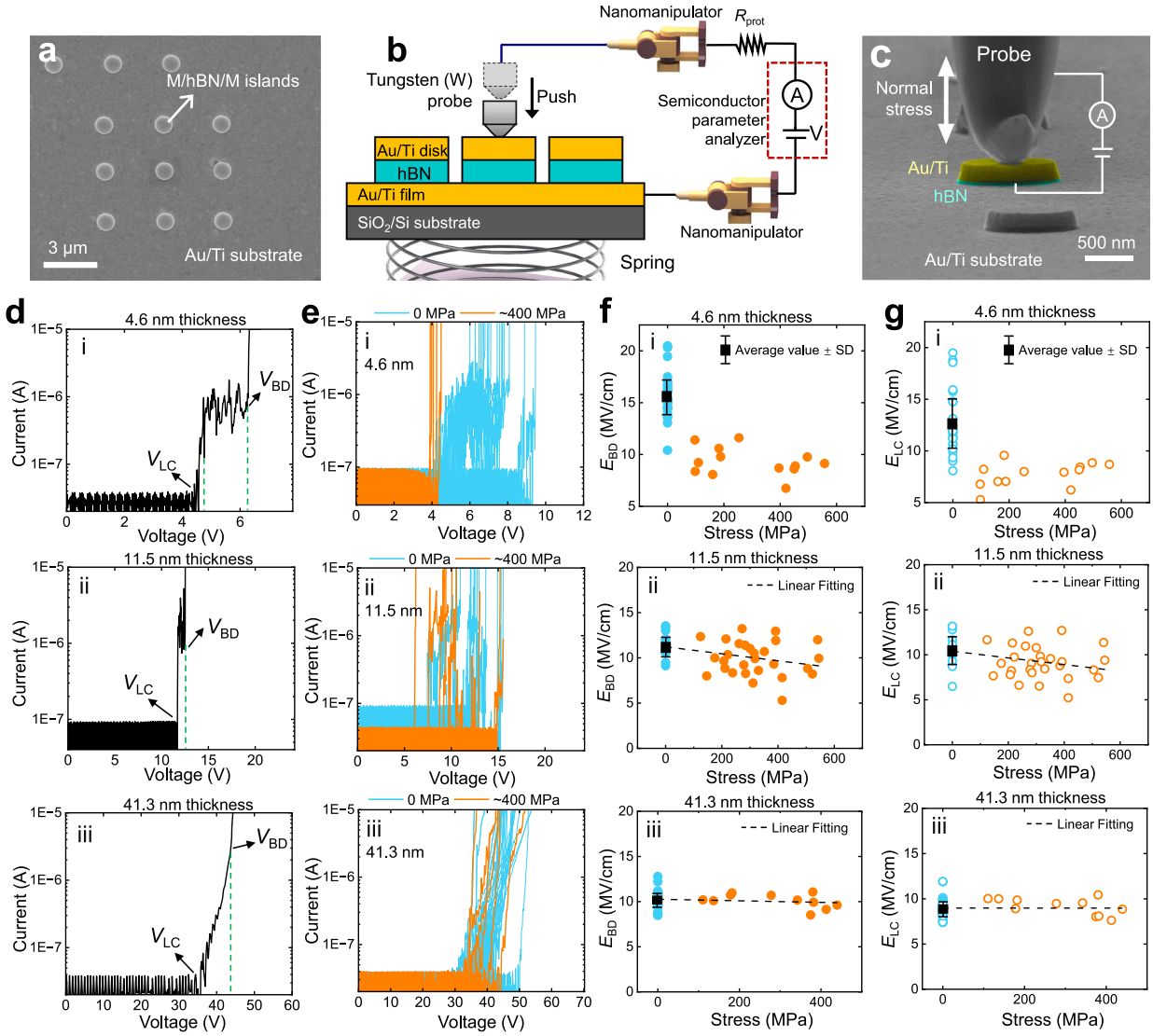

Fig. 1 | Experimental setup and multi-sample ramped voltage stress (RVS) tests on the dielectric strength of hBN nanosheets under mechanical stress. a SEM image showing the array of metal/hBN/metal (M/hBN/M) islands for dielectric strength tests. **b** Schematic drawing showing the measurement setup, where a metal/hBN/metal island is indented by a tungsten (W) probe, and the compression force is measured by the spring stage. **c** SEM image showing breakdown test on a metal/hBN/metal island indented by a W probe. Pseudo-colors were used to distinguish the metal film and hBN nanosheet. **d** Typical current (*I*)–voltage (*V*) curves of RVS tests for 4.6, 11.5, and 41.3 nm hBN nanosheets without mechanical stress. The voltage for the onset of leakage current is defined as V_{LC}, and the voltage for the onset of dielectric breakdown is defined as V_{BD}. **e** Repeatedly tested *I*–*V* curves of RVS tests for 4.6, 11.5, and 41.3 nm hBN nanosheets with 0 and ~400 MPa stress, respectively. Each *I*–*V* curve is measured from a different island sample (multi-sample RVS test). **f** The plots of breakdown strength (E_{BD}) as a function of stress for nanosheets of 4.6 nm (i), 11.5 nm (ii), and 41.3 nm (iii). **g** The plots of electric field strength (E_{LC}) corresponding to V_{LC} as a function of stress for nanosheets of 4.6, 11.5, and 41.3 nm. The number of island samples corresponding to the 4.6, 11.5, and 41.3 nm nanosheets is 37, 42, and 52, respectively. Each *I*–*V* curve or data point in figures **e**–**g** comes from a different island sample. The black squares represent the average E_{BD} or E_{LC} at zero stress, with the error bars represented by standard deviations (SD). The round dots and circles represent E_{BD} and E_{LC} under different stress. In figures for 11.5 and 41.3 nm, the dashed lines are linear fits of experimental data. Source data are provided as a Source Data file.

mechanical stress on the dielectric strength of hBN nanosheets, we performed RVS tests on the nanosheets of the three thicknesses under different normal stresses. Comparative *I*–*V* curves of RVS tests under zero and ~400 MPa normal stress are shown in Fig. 1e. Two phenomena are observed. First, *I*–*V* curves of different samples for each thickness show quite different V_{LC} and V_{BD} under zero stress, especially for those of thin nanosheets of 4.6 nm. Second, despite the scattering in V_{LC} and V_{BD} among different samples, *I*–*V* curves for thin nanosheets of 4.6 nm are obviously left shifted with smaller V_{LC} and V_{BD} when ~400 MPa normal stress is applied. In contrast, the normal stress causes a less obvious decrease of V_{LC} and V_{BD} for the nanosheets with 11.5 and 41.3 nm thickness.

To get insights into the effects of normal mechanical stress on dielectric strength of hBN nanosheets, E_{BD} and E_{LC} of hBN nanosheets are extracted from *I*–*V* curves of multi-sample RVS tests under different stress, as shown in Figure 1f and g. For those samples with the same thicknesses, E_{BD} and E_{LC} exhibit a similar dependence on normal mechanical stress, consistent with their roles as sequential indicators of dielectric breakdown. A small E_{LC} is generally associated with a small E_{BD}. For thin nanosheets with 4.6 nm thickness, E_{BD} and E_{LC} exhibit average values of 15.7 and 12.6 MV/cm, respectively, at zero normal stress. An E_{BD} as high as 15.7 MV/cm at zero stress indicates the high quality of our hBN nanosheets. The average values of 8.6 and 8.0 MV/cm around 400 MPa are obtained for E_{BD} and E_{LC},

https://doi.org/10.1038/s41467-025-63358-6

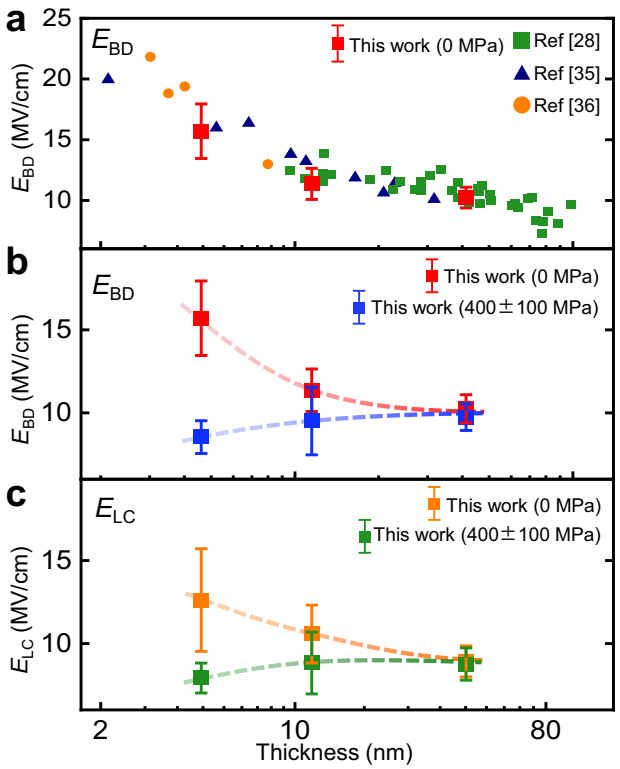

Fig. 2 | Summary of the breakdown strength E_{BD} and E_{LC} as a function of the thickness of hBN. a Comparison of E_{BD} at zero stress measured in this work with the data from previous reports[28,35,36]. The horizontal axis is the thickness of hBN. **b** Our measured E_{BD} in this work without stress (red square) and with the mechanical stress of 400 ± 100 MPa (blue square) at different thicknesses. **c** Our measured E_{LC} from 102 different samples in this work, without stress (yellow square) and with the mechanical stress of 400 ± 100 MPa (green square) at different thicknesses. The number of 4.6, 11.5, and 41.3 nm samples we tested without stress is 24, 14, and 41, respectively. The number of 4.6, 11.5, and 41.3 nm samples with the stress of 400 ± 100 MPa are 5, 12, and 6, respectively. The square points represent the average values of our measured E_{BD} or E_{LC} from different samples, and the error bars are represented with standard deviations. The dashed lines in (**b**) and (**c**) are guides for the eyes. Source data are provided as a Source Data file.

respectively. Both E_{BD} and E_{LC} show an overall decrease with the increase of normal stress, especially in the range of 0–200 MPa. For the nanosheets with 11.5 nm thickness, E_{BD} and E_{LC} exhibit average values of 11.4 and 10.6 MV/cm, respectively, at zero normal stress. Both E_{BD} and E_{LC} decrease slowly with the increase of normal stress with an overall rate of 0.38 MV/cm per 100 MPa in the range of 0–500 MPa. For thick hBN nanosheets with 41.3 nm thickness, E_{BD} and E_{LC} exhibit the average values of 10.2 and 8.9 MV/cm, respectively, at zero normal stress, and show a negligible decrease with the increase of normal stress.

To display the thickness-dependent dielectric strength weakening of 2D hBN, the presently measured E_{BD} of hBN nanosheets evolving with different thicknesses are shown in Fig. 2 together with those in the previous reports[28,35,36]. As shown in Fig. 2a, thicker nanosheets are found to have smaller E_{BD} at zero normal stress. Both the value of E_{BD} at zero normal stress measured in our work and its dependence on thickness agree well with those in the previous reports. It can be seen from Fig. 2b, c that the breakdown strength of hBN nanosheets with 4.6 and 11.5 nm thickness is obviously weakened by the normal mechanical stress of about 400 MPa, with more significant weakening for thinner nanosheets, while thick hBN nanosheets with 41.3 nm thickness can retain their breakdown strength under the normal stress up to about 400 MPa in multi-sample RVS tests.

The dielectric strength of hBN nanosheets shows obvious randomness among different samples, as shown in Fig. 1. To obtain the dielectric strength of hBN nanosheets statistically, the breakdown strength of hBN nanosheets is analyzed by cluster fitting (see Fig. S7 in Supplementary Information)[44,45], which can give the characteristic strength of electric field ($E_{63.2\%}$) corresponding to cumulative breakdown probability of 63.2%. At zero mechanical stress, the nanosheets with 4.6, 11.5, and 41.3 nm thickness show $E_{63.2\%}$ of 15.1, 11.0, and 10.4 MV/cm, respectively. This is in good agreement with the varying trend of average E_{BD} with thickness as shown in Fig. 2a. In contrast, when mechanical stress of ~400 MPa is applied, $E_{63.2\%}$ decreases to 8.9, 10.1, and 9.5 MV/cm, respectively. In agreement with the average breakdown strength, $E_{63.2\%}$ is weakened by mechanical stress, with thinner nanosheets showing more remarkable weakening. While the nanosheets with 4.6 nm thickness show larger $E_{63.2\%}$ than that of 11.5 and 41.3 nm nanosheets at zero normal stress, they show smaller $E_{63.2\%}$ than that of the latter at ~400 MPa normal stress.

Despite negligible effects on the E_{BD} and E_{LC} of 41.3 nm-thick hBN nanosheets in multi-sample RVS tests, normal mechanical stress is found to have a critical effect on leakage current of the thick nanosheets in single-sample RVS tests. A single-sample RVS test is to perform RVS measurements repeatedly on the same island sample to assess its dielectric strength over multiple cycles. As shown in Fig. S8, single-sample RVS tests on thicker hBN samples generally show two different phenomena: hard breakdown with irreversible dielectric performance, and soft breakdown with reversible dielectric performance. Since a hard breakdown causes all subsequent RVS cycles to follow the same short circuit in I–V curves, single-sample RVS tests with soft breakdown are employed to observe the continuous evolution of leakage current and dielectric strength of hBN nanosheets.

Figure 3a and b show the sequential I–V curves of single-sample RVS tests on 41.3 nm nanosheets with the normal stress of 0 and 490 MPa, respectively. Repeated RVS tests were performed for 14 and 13 cycles, respectively. E_{BD} and E_{LC} of the I–V curves and their difference $\Delta E = E_{BD} - E_{LC}$ are shown in Fig. 3c and d. Two phenomena are observed. First, repeated RVS tests at the same point of a sample result in smaller and smaller E_{LC} and no obvious decrease in E_{BD} for both 0 and 490 MPa normal stress. Leakage current, therefore, appears at smaller and smaller voltages for repeated RVS tests. Second, the normal stress can speed up the reduction of E_{LC} and significantly increase the leakage current. While ΔE increases to 4.26 MV/cm after 14 repeated RVS tests with zero normal stress, ΔE increases to 10.72 MV/cm for 13 repeated tests with 490 MPa normal stress. Importantly, E_{LC} decreases by more than 10 times to <1 MV/cm, and leakage current can progressively increase to 10 μA before the breakdown, which is one order of magnitude larger than that (<1 μA) with zero stress, after repeated RVS tests for more than 10 times in the latter case. The results indicate that normal mechanical stress can significantly degrade the ability of hBN nanosheets to block leakage current in cyclic voltage application, even for thick nanosheets up to 41.3 nm.

Dielectric strength weakening in constant voltage stress tests

The dielectric strength of hBN nanosheets is then studied by constant voltage stress (CVS) tests, where electrical current across the metal/hBN/metal structure under a fixed voltage is recorded with time. Notably, since E_{BD} varies with the thickness of samples as shown in Fig. 2, applying the same strength of the electric field to the samples with different thicknesses will result in quite different behaviors of leakage current: while thick samples with lower E_{BD} exhibit instantaneous dielectric breakdown, thin samples with higher E_{BD} exhibit negligible leakage current for a long time (>2000 s). In order to focus on the effect of mechanical stress on leakage current, we chose a specific voltage slightly less than the V_{BD} to each sample to obtain current (I)–time (T) curves within a reasonable time (typically <1000 s),

https://doi.org/10.1038/s41467-025-63358-6

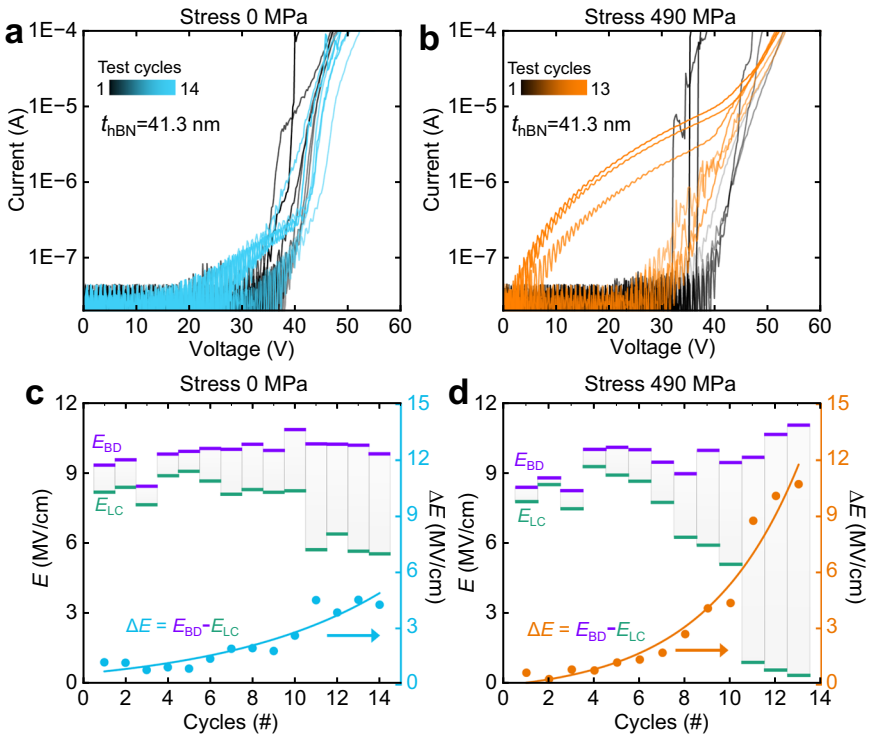

Fig. 3 | Single-sample RVS tests on the dielectric strength of hBN nanosheets under mechanical stress. a, **b** Sequential *I*–*V* curves of single-sample RVS tests on the dielectric strength of 41.3 nm-thick nanosheets with 0 MPa (**a**) and 490 MPa (**b**) stress. In single-sample RVS tests, repeated RVS tests are performed on the same island sample. **c**, **d** E_{BD} (purple horizontal lines), E_{LC} (green horizontal lines), and their difference ($\Delta E = E_{BD}$–E_{LC}, solid points) of the sequential *I*–*V* curves of single-sample RVS tests in **a** (**c**) and **b** (**d**). The solid lines in **c** and **d** are the exponential fitting of ΔE. Source data are provided as a Source Data file.

which not only ensures us to observe obvious leakage current but also does not induce immediate breakdown.

Typical *I*–*T* curves of CVS tests for hBN nanosheets with different thicknesses and under different normal stresses are shown in Fig. 4a–c. Each *I*–*T* curve is measured from a different island sample (multi-sample CVS tests). Four phenomena are observed in Fig. 4a–d. First, remarkable leakage current can be observed after a period of time (defined as T_{LC}) even though the applied voltage is smaller than V_{BD}. In addition to the strength of the electric field, the applied duration of the electric field therefore contributes to the dielectric strength degradation of hBN nanosheets, which agrees well with previous reports[39,46]. Therefore, an electric voltage smaller than V_{BD} may induce remarkable leakage current after a long duration of voltage application. This character will cause a serious problem to the long-term reliability of hBN nanosheet-based devices. Second, the onset of leakage current of thin nanosheets with thicknesses of 4–6 and 10–13 nm under fixed voltage can be significantly accelerated by normal stress with smaller T_{LC} (Fig. 4a, b). For the thin samples with a thickness of 4–6 nm, T_{LC} can be shortened from around 500 s to <20 s when a stress of about 600 MPa is applied. Third, the stress-induced acceleration of the onset of leakage current is more significant for thinner samples. Figure 4d shows the T_{LC} extracted from more than 20 CVS tests under different stress conditions in Fig. 4a, b. While 4–6 nm-thick samples exhibit a decreasing rate of T_{LC} being about 0.9 s/MPa, 10–13 nm-thick samples exhibit a smaller decreasing rate of about 0.6 s/MPa. Fourth, mechanical stress shows no regular effect on the onset of leakage current of thick samples with a thickness of 37–42 nm (Fig. 4c), indicating that the effect of mechanical stress on the onset of leakage current is negligible for such thick nanosheets.

In addition to multi-sample CVS tests, single-sample CVS tests are also performed to investigate the effect of normal stress on the leakage current of hBN nanosheets. In single-sample CVS tests, *I*–*T* curves under different normal stresses are recorded from the same samples. Figure 4e, f show the *I*–*T* curves of two different samples in 8.9 nm thickness when they were stressed and unstressed. It can be seen that both the magnitude of the leakage current and its increasing rate with time are significantly increased when subjected to normal stress. As indicated by the red dashed lines in Fig. 4f, the *I*–*T* curves near the onset of obvious leakage currents can be described by the power law $I \propto (T - T_{LC})^C$, where *C* is the exponent used to measure the increased rate of leakage current, similar to that of voltage stress-induced leakage current (SILC) in the previous reports[47]. In addition to smaller T_{LC}, it can be seen that both samples exhibit larger *C* when they are loaded, indicating a larger increasing rate of leakage current under normal stress. Therefore, both multi-sample and single-sample CVS tests indicate that normal mechanical stress can weaken the dielectric strength of thin hBN nanosheets by inducing larger leakage current and a faster increase of leakage current.

Mechanism for thickness-dependent dielectric strength weakening

Both RVS and CVS tests demonstrate the mechanical stress-induced dielectric strength weakening of hBN nanosheets, with thinner nanosheets showing more obvious weakening. Mechanical stress-induced dielectric strength weakening has been observed in traditional dielectrics. Zeller and Steve et al. have found that mechanical stress can effectively reduce the breakdown strength of SiO_2 films[25,48]. They have speculated that the effects of electric field and mechanical stress on breakdown failure in dielectrics are basically the same, and failure occurs when the local electric field and mechanical stress accumulate to a limit. Recently, Mario et al. reported that the pressure applied by the probe on the top of the metal/insulator/metal (MIM) memristor can reduce the breakdown voltage[49]. In the study of dielectric ceramics, Li et al. calculated the von Mises stress distribution and mentioned that strain reduces the breakdown electric field by promoting microcrack initiation and accelerating local discharge[50].

https://doi.org/10.1038/s41467-025-63358-6

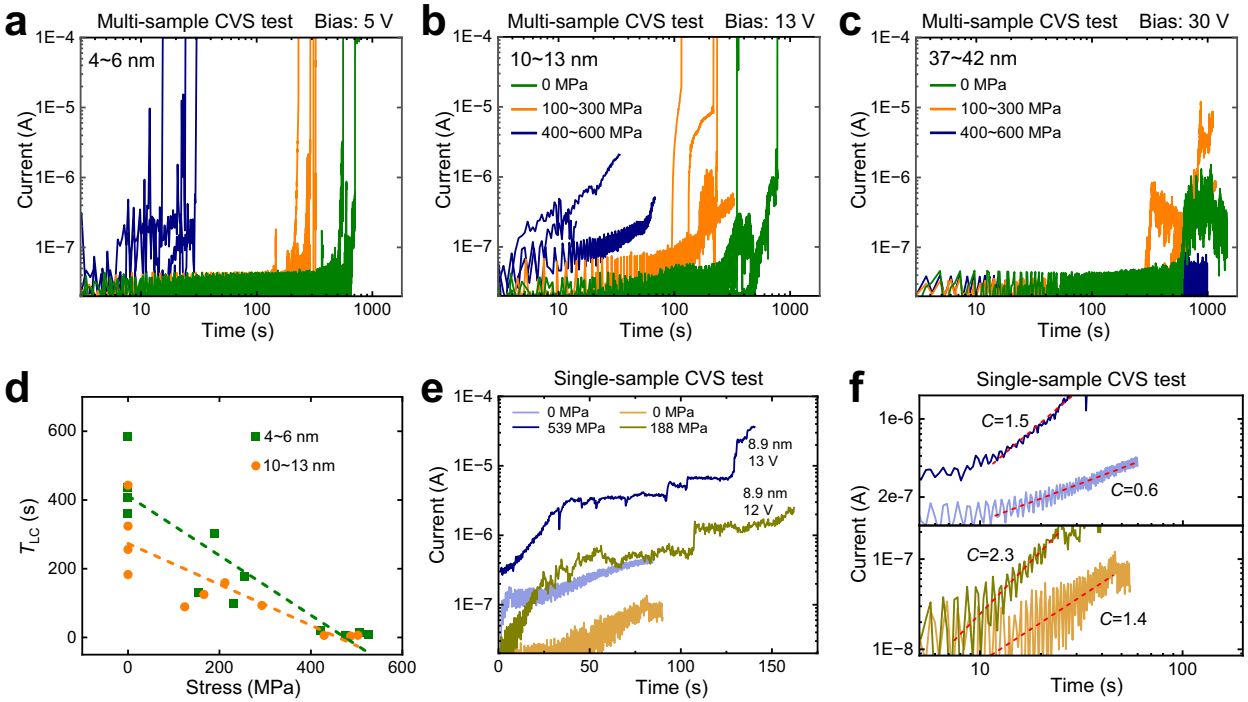

Fig. 4 | Constant voltage stress (CVS) tests on the dielectric strength of hBN nanosheets under mechanical stress. a–c Current (*I*)–time (*T*) curves of multi-sample CVS tests on hBN nanosheets with thicknesses of (**a**) 4–6 nm, (**b**) 10–13 nm, and (**c**) 37–42 nm when different stress is applied. The green, yellow, and blue curves correspond to the stress range of 0, 100–300, and 400–600 MPa, respectively. The time for the onset of the obvious leakage current is defined as T_{LC}. **d** The plots of T_{LC} in (**a**) and **b** versus stress for hBN nanosheets with 4–6 and 10–13 nm. The dashed lines are a linear fit of the data points. **e** *I*–*T* curves of single-sample CVS tests on 8.9 nm-thick hBN nanosheets when they are stressed (dark blue/yellow lines for 13/12 V) and unstressed (light blue/yellow lines for 13/12 V). **f** *I*–*T* curves zoomed in near the onset of obvious leakage current in (**e**). The red dashed lines are power function fitting of *I*–*T* curves with the formula $I = A(T-T_{LC})^C$, where *A* and *C* are constants. The value of *C* is shown for each curve. Source data are provided as a Source Data file.

Along with traditional dielectric research, the electro-fracture mechanics model[48] and the filamentary electromechanical breakdown model[51] based on fracture mechanics have been proposed and continuously improved. Regarding stress-induced overall compression in thickness and subsequent strength enhancement of the electric field, the thickness compression of hBN nanosheets is calculated to be less than about 2% (see Section 9 of Supplementary Information). Such a small thickness compression cannot make hBN show remarkable dielectric strength weakening by the enhancing strength of the electric field.

So, what is the mechanism responsible for the mechanical stress-induced dielectric strength weakening in the 2D hBN? Progressive breakdown of hBN under an electric field can be attributed to various mechanisms, including anode hole injection[52], anode hydrogen release[53], atomic migration[54], collision ionization[55], and so on. These defect-based factors are directly related to the application of the electric field and the subsequent flow of electrical current, so we therefore summarize them as the electric field-induced defects. Dielectric breakdown of hBN without mechanical stress is directly related to the formation and accumulation of the electric field-induced defects. Similar to an electric field, mechanical stress can induce defects in 2D materials from the atomic level to the crystallographic level, including lattice deformation[56], dislocations[57], and cracks[58]. In addition to the above defects induced by mechanical stress, mechanical stress may accelerate the aggregation and expansion of pre-existing electric field-induced defects[59,60]. We here refer to all these mechanical factors that are likely to cause dielectric breakdown as mechanical stress-induced defects. The mechanical stress-induced defects are expected to result in dielectric breakdown in a similar way to that of electric field-induced defects. When an hBN nanosheet is subjected to both electric field and mechanical stress, the effects of electric field and mechanical stress on dielectric breakdown will be coupled together and superimposed, showing accelerated breakdown compared with the case without mechanical stress. Therefore, mechanical stress-induced dielectric strength weakening in 2D hBN is attributed to accelerated formation and accumulation of defects by mechanical stress.

To further illustrate the mechanism responsible for the thickness-dependent dielectric strength weakening in 2D hBN, we conducted FEM simulations to study the internal stress distribution in hBN nanosheets. Figure 5a shows the distribution of the von Mises stress, which is closely related to the defect accumulation and failure of materials[61], in 40 nm-thick hBN nanosheets. It can be seen that the stressed area in the hBN nanosheet is larger than that where uniaxial stress is applied because of the bending stiffness of the top metal layer. Importantly, the stress at the bottom surface of the nanosheets is smaller than that at the upper surface, indicating a stress gradient in the thickness direction. The gradual attenuation of stress is caused by the gradual expansion of the stressed area from the top to the bottom and is found to be strongly dependent on the thickness. The ratio of the stress at the bottom surface (P_{bottom}) to that at the upper surface (P_{top}) is found to decrease with the thickness increase (Fig. 5b). P_{bottom}/P_{top} of the von Mises stress is 73.3% for a 4 nm-thick nanosheet and decreases to 35.0% for a 40 nm-thick nanosheet. The ratio of normal stress (S_{33}) shows a similar decrease with the increase in thickness. The thickness-dependent stress gradient is thought to be responsible for the thickness-dependent dielectric strength weakening.

Dielectric breakdown of hBN nanosheets under mechanical stress is schematically shown in Fig. 5c. For thin nanosheets, internal stress accumulation and mechanical stress-induced defects (see green dots) show similar density across the thickness because of a small mechanical stress gradient, so the progressive breakdown across the thickness

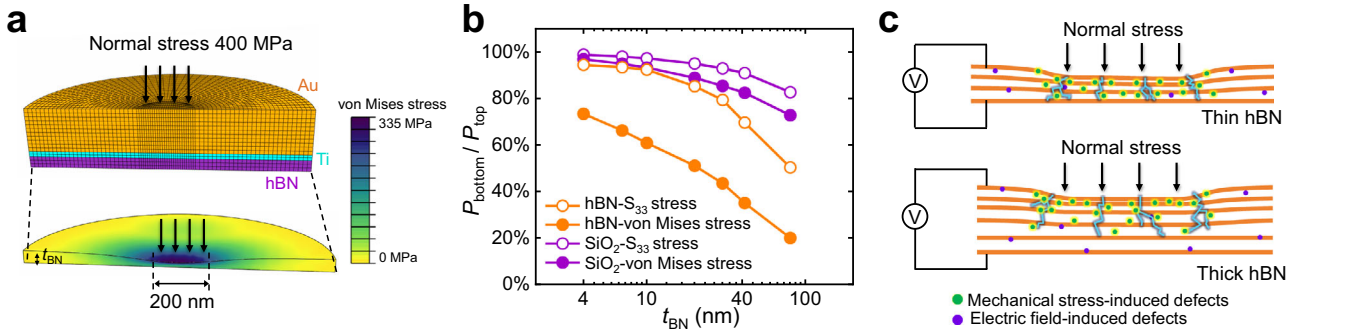

Fig. 5 | Simulation of mechanical stress in hBN nanosheets. a Cloud diagram of von Mises stress distribution in a hBN nanosheet with 40 nm thickness based on finite element method (FEM) simulation. In the simulation, an island sample with the same metal/hBN/metal structure as that in our experiments is indented with 400 MPa pressure in the center area with 200 nm in diameter, similar to that in our experiments. **b** The ratio of the simulated stress at the bottom surface (P_{bottom}) to that at the upper surface (P_{top}) of hBN and SiO_2 nanosheets with different thicknesses. Both von Mises stress (solid dots) and the *c*-axis S_{33} stress (hollow dots) are displayed. Source data are provided as a Source Data file. **c** Schematic drawing showing dielectric breakdown (meandering lines) in thin (upper figure) and thick (bottom figure) hBN nanosheets under electric field and mechanical stress. The defects induced by the electric field and mechanical stress are represented by purple and green dots, respectively.

can be easily sped up by mechanical stress. In contrast, for thick nanosheets, the internal stress and mechanical stress-induced defects near the bottom surface are much smaller than those near the upper surface because of the large internal stress gradient. So, compared with thin nanosheets, it is more difficult to achieve dielectric breakdown across the whole thickness under mechanical stress in thick nanosheets. Thicker nanosheets are less susceptible to the mechanical stress-induced dielectric strength weakening. Thickness-dependent dielectric strength weakening observed in our experiments can therefore be well explained by the mechanism that internal stress accelerates the formation and accumulation of defects in 2D hBN and thus accelerates the breakdown process. This further supports the proposed mechanism for mechanical stress-induced dielectric strength weakening in 2D hBN.

Importantly, the attenuation of internal stress along the thickness direction is closely related to the layered structure of hBN nanosheets. For comparison, we calculate the stress distribution in isotropic SiO_2 thin films with different thicknesses (Figs. 5b and S9). Even though stress attenuation is also observed in SiO_2 films, hBN exhibits much more obvious attenuation of mechanical stress than that of SiO_2, especially in von Mises stress. When the thickness increases from 4 to 40 nm, similar to that in our experiments, P_{bottom}/P_{top} of the von Mises stress in SiO_2 decreases from 96.7% to 82.3%, while it decreases from 73.3% to 35.0% in hBN. In addition to the more obvious attenuation of von Mises stress in hBN for a specific thickness, stress attenuation in hBN also exhibits a stronger thickness dependence than that in SiO_2. The phenomena are attributed to the larger lateral expansion of stressed areas in anisotropic layered structures than that in isotropic SiO_2. Our observed thickness-dependent dielectric strength weakening of hBN nanosheets under mechanical stress is therefore closely related to their layered structures.

In summary, the dielectric strength of hBN nanosheets under mechanical stress is systematically studied by multi-sample/single-sample RVS/CVS tests. The dielectric strength of hBN nanosheets is found to be weakened with lower breakdown strength, shorter breakdown time and larger leakage current under normal mechanical stress. The dielectric strength weakening is found to show thickness dependence, with more remarkable weakening for thinner nanosheets, which is closely related to the layered structures of hBN nanosheets. The ability of hBN nanosheets to block leakage current in cyclic voltage application can be significantly degraded by mechanical stress, even for thick nanosheets up to 41.3 nm. The results indicate that hBN nanosheets are not ideal insulators for 2D material-based devices exposed to mechanical stress, and special cautions are needed in cases with possible mechanical stress, especially for those on flexible substrates.

Methods

Sample preparation

Au/Ti film (thickness 200/20 nm) is firstly deposited on SiO_2/Si substrate (~285 nm/500 μm in thickness) using electron beam evaporation (Texas Instruments DE400) method. High-quality hBN nanosheets with different thicknesses (<50 nm) are obtained by the mechanical exfoliation method from hBN bulk crystals synthesized by the high-pressure high-temperature method[62] and transferred to the substrate with an Au film using thermal-release tape. The thickness of hBN nanosheets is measured by atomic force microscopy (AFM). hBN nanosheets with uniform thickness in a large area are selected under an optical microscope. An array of Au/Ti metal disks with a thickness of 160/20 nm and a diameter of 1 μm is prepared on the surface of the hBN nanosheets using microfabrication techniques, including electron beam lithography (Raith150 Two), electron beam evaporation, and lift-off process. The array of metal/hBN/metal islands is obtained by etching away hBN surrounding the metal disks through reactive ion etching (ETCHLAB 200) (O_2/CHF_3, 4/40 sccm, 60 W, 5 min) using the metal disks as the marks (see Fig. S2 in Supplementary Information).

Dielectric strength tests under mechanical stress

Dielectric strength tests are performed at room temperature inside the vacuum chamber (~10^{-3} Pa) of an SEM (FEI Quanta 600F) equipped with two nanomanipulators (Kleindiek MM3A). The substrate with an array of metal/hBN/metal islands is fixed to a spring stage that is held by a nanomanipulator. A tungsten (W) probe held by another nanomanipulator is manipulated to indent a metal/hBN/metal island to apply normal mechanical pressure to the hBN nanosheets. Electrical voltage and current of metal/hBN/metal islands are sourced and measured by using a semiconductor parameter analyzer (Keithley 4200-SCS) through the two nanomanipulators.

Reporting summary

Further information on research design is available in the Nature Portfolio Reporting Summary linked to this article.

Data availability

All raw data generated during the study are available from the corresponding author upon request. Source data are provided with this paper.

References

1. Knobloch, T. et al. The performance limits of hexagonal boron nitride as an insulator for scaled CMOS devices based on two-dimensional materials. *Nat. Electron.* **4**, 98–108 (2021).
2. Sasama, Y. et al. High-mobility p-channel wide-bandgap transistors based on hydrogen-terminated diamond/hexagonal boron nitride heterostructures. *Nat. Electron.* **5**, 37–44 (2022).
3. Dean, C. R. et al. Boron nitride substrates for high-quality graphene electronics. *Nat. Nanotechnol.* **5**, 722–726 (2010).
4. Dean, C. R. et al. Multicomponent fractional quantum Hall effect in graphene. *Nat. Phys.* **7**, 693–696 (2011).
5. Wang, J. et al. High mobility MoS_2 transistor with low Schottky barrier contact by using atomic thick h-BN as a tunneling layer. *Adv. Mater.* **28**, 8302–8308 (2016).
6. Britnell, L. et al. Field-effect tunneling transistor based on vertical graphene heterostructures. *Science* **335**, 947–950 (2012).
7. Purdie, D. G. et al. Cleaning interfaces in layered materials heterostructures. *Nat. Commun.* **9**, 5387 (2018).
8. Wang, L. et al. One-dimensional electrical contact to a two-dimensional material. *Science* **342**, 614–617 (2013).
9. Cao, Y. et al. Correlated insulator behaviour at half-filling in magic-angle graphene superlattices. *Nature* **556**, 80–84 (2018).
10. Chen, G. et al. Signatures of tunable superconductivity in a trilayer graphene moiré superlattice. *Nature* **572**, 215–219 (2019).
11. Yankowitz, M., Ma, Q., Jarillo-Herrero, P. & LeRoy, B. J. van der Waals heterostructures combining graphene and hexagonal boron nitride. *Nat. Rev. Phys.* **1**, 112–125 (2019).
12. Zeng, S., Liu, C. & Zhou, P. Transistor engineering based on 2D materials in the post-silicon era. *Nat. Rev. Electr. Eng.* **1**, 335–348 (2024).
13. Yang, Q. et al. Steep-slope vertical-transport transistors built from sub-5 nm Thin van der Waals heterostructures. *Nat. Commun.* **15**, 1138 (2024).
14. Akinwande, D., Petrone, N. & Hone, J. Two-dimensional flexible nanoelectronics. *Nat. Commun.* **5**, 5678 (2014).
15. Sangwan, V. K. & Hersam, M. C. Neuromorphic nanoelectronic materials. *Nat. Nanotechnol.* **15**, 517–528 (2020).
16. Jin, C. et al. Interlayer electron–phonon coupling in WSe_2/hBN heterostructures. *Nat. Phys.* **13**, 127–131 (2017).
17. Geim, A. K. & Grigorieva, I. V. Van der Waals heterostructures. *Nature* **499**, 419–425 (2013).
18. Shimazaki, Y. et al. Strongly correlated electrons and hybrid excitons in a moiré heterostructure. *Nature* **580**, 472–477 (2020).
19. Khestanova, E., Guinea, F., Fumagalli, L., Geim, A. K. & Grigorieva, I. V. Universal shape and pressure inside bubbles appearing in van der Waals heterostructures. *Nat. Commun.* **7**, 12587 (2016).
20. Bera, K., Chugh, D., Tan, H. H., Roy, A. & Jagadish, C. Non-thermal and thermal effects on mechanical strain in substrate-transferred wafer-scale hBN films. *J. Appl. Phys.* **132**, 104303 (2022).
21. Kriegel, M. A., Omambac, K. M., Franzka, S., Meyer zu Heringdorf, F.-J. & Horn-von Hoegen, M. Incommensurability and negative thermal expansion of single layer hexagonal boron nitride. *Appl. Surf. Sci.* **624**, 157156 (2023).
22. Tang, Z. et al. A steep-slope MoS_2/graphene Dirac-source field-effect transistor with a large drive current. *Nano Lett.* **21**, 1758–1764 (2021).
23. Lee, G.-H. et al. Flexible and transparent MoS_2 field-effect transistors on hexagonal boron nitride–graphene heterostructures. *ACS Nano* **7**, 7931–7936 (2013).
24. Georgiou, T. et al. Vertical field-effect transistor based on graphene–WS_2 heterostructures for flexible and transparent electronics. *Nat. Nanotechnol.* **8**, 100–103 (2013).
25. Jeffery, S., Sofield, C. J. & Pethica, J. B. The influence of mechanical stress on the dielectric breakdown field strength of thin SiO_2 films. *Appl. Phys. Lett.* **73**, 172–174 (1998).
26. Choi, Y. S., Park, H., Nishida, T. & Thompson, S. E. Reliability of HfSiON gate dielectric silicon MOS devices under [110] mechanical stress: time dependent dielectric breakdown. *J. Appl. Phys.* **105**, 044503 (2009).
27. Cho, C. et al. Strain-resilient electrical functionality in thin-film metal electrodes using two-dimensional interlayers. *Nat. Electron.* **4**, 126–133 (2021).
28. Hattori, Y., Taniguchi, T., Watanabe, K. & Nagashio, K. Comparison of device structures for the dielectric breakdown measurement of hexagonal boron nitride. *Appl. Phys. Lett.* **109**, 253111 (2016).
29. Cook, J. T. et al. Temperature-dependent dielectric properties of polyimide (PI) and polyamide (PA) nanocomposites. *IEEE Trans. Nanotechnol.* **20**, 584–591 (2021).
30. Zhou, J. et al. Temperature-dependent breakdown and pre-breakdown conduction of polyethylene terephthalate. *J. Phys. D: Appl. Phys.* **55**, 365302 (2022).
31. Luan, B. & Robbins, M. O. The breakdown of continuum models for mechanical contacts. *Nature* **435**, 929–932 (2005).
32. Stifter, T., Marti, O. & Bhushan, B. Theoretical investigation of the distance dependence of capillary and van der Waals forces in scanning force microscopy. *Phys. Rev. B* **62**, 13667–13673 (2000).
33. Day, H. C. & Allee, D. R. Selective area oxidation of silicon with a scanning force microscope. *Appl. Phys. Lett.* **62**, 2691–2693 (1993).
34. Avouris, P., Martel, R., Hertel, T. & Sandstrom, R. AFM-tip-induced and current-induced local oxidation of silicon and metals. *Appl. Phys. A* **66**, S659–S667 (1998).
35. Hattori, Y., Taniguchi, T., Watanabe, K. & Nagashio, K. Layer-by-layer dielectric breakdown of hexagonal boron nitride. *ACS Nano* **9**, 916–921 (2015).
36. Ranjan, A. et al. Dielectric breakdown in single-crystal hexagonal boron nitride. *ACS Appl. Electron. Mater.* **3**, 3547–3554 (2021).
37. Shi, Y. et al. Electronic synapses made of layered two-dimensional materials. *Nat. Electron.* **1**, 458–465 (2018).
38. Pan, C. et al. Coexistence of grain-boundaries-assisted bipolar and threshold resistive switching in multilayer hexagonal boron nitride. *Adv. Funct. Mater.* **27**, 1604811 (2017).
39. Ranjan, A. et al. Molecular bridges link monolayers of hexagonal boron nitride during dielectric breakdown. *ACS Appl. Electron. Mater.* **5**, 1262–1276 (2023).
40. Shen, Y. et al. Two-dimensional-materials-based transistors using hexagonal boron nitride dielectrics and metal gate electrodes with high cohesive energy. *Nat. Electron.* **7**, 856–867 (2024).
41. Wang, B. et al. Large and pressure-dependent c-axis piezoresistivity of highly oriented pyrolytic graphite near zero pressure. *Nano Lett.* **24**, 4965–4971 (2024).
42. Li, J., Zhang, G., Wang, L. & Dai, Z. Indentation of a plate on a thin transversely isotropic elastic layer. *Acta Mech. Solida Sin.* **38**, 331–340 (2024).
43. Palumbo, F. et al. A review on dielectric breakdown in thin dielectrics: silicon dioxide, high-*K*, and layered dielectrics. *Adv. Funct. Mater.* **30**, 1900657 (2020).
44. Shimizu, T. et al, A new aspect of time-dependent clustering model for non-uniform dielectric TDDB. *2016 IEEE International Reliability Physics Symposium (IRPS)*, pp. 3A-4-1-3A-4-10 (IEEE, Pasadena, CA, USA, 2016)
45. Beek, S. V. et al. Four point probe ramped voltage stress as an efficient method to understand breakdown of STT-MRAM MgO tunnel junctions. *2015 IEEE International Reliability Physics Symposium (IRPS)*, pp. MY.4.1-MY.4.6 (IEEE, Monterey, CA, USA, 2015).
46. Pazos, S. et al. High-temporal-resolution characterization reveals outstanding random telegraph noise and the origin of dielectric breakdown in h-BN memristors. *Adv. Funct. Mater.* **34**, 2213816 (2024).
47. Mannequin, C. et al. Stress-induced leakage current and trap generation in HfO_2 thin films. *J. Appl. Phys.* **112**, 074103 (2012).

48. Zeller, H. R. & Schneider, W. R. Electrofracture mechanics of dielectric aging. *J. Appl. Phys.* **56**, 455–459 (1984).
49. Zuo, Y. et al. Effect of the pressure exerted by probe station tips in the electrical characteristics of memristors. *Adv. Electron. Mater.* **6**, 1901226 (2020).
50. Li, J. et al. Grain-orientation-engineered multilayer ceramic capacitors for energy storage applications. *Nat. Mater.* **19**, 999–1005 (2020).
51. Fothergill, J. C. Filamentary electromechanical breakdown. *IEEE Trans. Electr. Insul.* **26**, 1124–1129 (1991).
52. Hattori, Y., Taniguchi, T., Watanabe, K. & Nagashio, K. Impact ionization and transport properties of hexagonal boron nitride in a constant-voltage measurement. *Phys. Rev. B* **97**, 045425 (2018).
53. Hattori, Y., Taniguchi, T., Watanabe, K. & Nagashio, K. Anisotropic dielectric breakdown strength of single crystal hexagonal boron nitride. *ACS Appl. Mater. Interfaces* **8**, 27877–27884 (2016).
54. Jiang, L. et al. Dielectric breakdown in chemical vapor deposited hexagonal boron nitride. *ACS Appl. Mater. Interfaces* **9**, 39758–39770 (2017).
55. Guiot, V. et al. Avalanche breakdown in $GaTa_4Se_{8-x}Te_x$ narrow-gap Mott insulators. *Nat. Commun.* **4**, 1722 (2013).
56. Rooney, A. P. et al. Anomalous twin boundaries in two dimensional materials. *Nat. Commun.* **9**, 3597 (2018).
57. Ly, T. H., Zhao, J., Cichocka, M. O., Li, L.-J. & Lee, Y. H. Dynamical observations on the crack tip zone and stress corrosion of two-dimensional MoS_2. *Nat. Commun.* **8**, 14116 (2017).
58. Yang, Y. et al. Intrinsic toughening and stable crack propagation in hexagonal boron nitride. *Nature* **594**, 57–61 (2021).
59. Kruv, A. et al. On the impact of mechanical stress on gate oxide trapping. *2020 IEEE International Reliability Physics Symposium (IRPS)*, pp. 1-5 (IEEE, Dallas, TX, USA, 2020).
60. Schneider, G. A. Influence of electric field and mechanical stresses on the fracture of ferroelectrics. *Annu. Rev.* **37**, 491–538 (2007).
61. Vinod, S. et al. Low-density three-dimensional foam using self-reinforced hybrid two-dimensional atomic layers. *Nat. Commun.* **5**, 4541 (2014).
62. Taniguchi, T. & Watanabe, K. Synthesis of high-purity boron nitride single crystals under high pressure by using Ba–BN solvent. *J. Crystallogr. Growth* **303**, 525–529 (2007).

Acknowledgements

This work was supported by the National Natural Science Foundation of China (Grant Nos. 62350040 and 11890671). The authors acknowledge the support of the Nanofabrication Laboratory of Peking University. K.W. and T.T. acknowledge support from the JSPS KAKENHI (Grant Nos. 21H05233 and 23H02052) and World Premier International Research Center Initiative (WPI), MEXT, Japan.

Author contributions

X.W. conceived the idea and supervised the investigation. B.W., X.W., and Q.C. designed the experiments. B.W. fabricated the devices and performed dielectric strength measurements. B.W., C.Y. and Z.D. performed FEM simulations and analysis. Y.J., M.L. and W.W. contributed to device fabrication. C.T. contributed useful discussions. J.T., C.Y. and S.L. took TEM and AFM images. Z.F. facilitated the force measurement. T.T. and K.W. provided bulk hBN crystals. X.W., B.W. and Q.C. wrote the manuscript. All the authors read the manuscript and provided comments.

Competing interests

The authors declare no competing interests.

Additional information

Supplementary information The online version contains supplementary material available at https://doi.org/10.1038/s41467-025-63358-6.

Correspondence and requests for materials should be addressed to Xianlong Wei.

Peer review information *Nature Communications* thanks Mark Bissett, and the other, anonymous, reviewer(s) for their contribution to the peer review of this work. A peer review file is available.